CHAPTER 2:
SEMICONDUCTOR DETECTORS

2.1 Some basic properties of semiconductors

Semiconductors are mono-crystalline materials whose outer atomic shell levels exhibit an energy band structure. Energy states are concentrated into a valence band and a conduction band, separated by a gap where no energy states are allowed.

In insulators, the energy states in the valence band are completely filled while the conduction band is empty. The energy gap is sufficiently large so that thermal energy or an applied electrical field will not raise electrons from the valence band to the conduction band.

In conductors, the conduction band is either partially filled or overlaps with the valence band. The energy gap is very small or nonexistent. Electrons in the conduction band are called charge carriers and are free to move in the crystal lattice. If an electric field is applied current will flow in the conductor.

In a semiconductor, the energy gap is intermediate in size. Thermal energy is then sufficient to excite a few electrons from the valence band to the conduction band creating electron-hole pairs. Without an external electric field, electrons and holes recombine and equilibrium is established. With an electric field, the electrons and holes will undergo a net migration and a small current is observed.

2.1.1 Charge carrier mobility

Under low-to-moderate electric field, the drift velocity of the charge carriers in the semiconductor is proportional to a mobility "μ" constant and the magnitude of the applied field, "E".

$$v = \mu \cdot E \tag{2.1}$$

The mobility constant is roughly of the same order for electrons and holes, with electrons drifting slightly faster than the holes. Numerical values for Silicon and Germanium are given in Appendix B. At higher electric fields (above *1000 V/cm* at room temperature), the drift velocity increases more slowly reaching a saturation point, where it becomes independent of the electric field. The saturation occurs because at higher velocities, part of the kinetic energy is lost by collisions with the lattice atoms. In the Silicon drift detector, which is the focus of this thesis, the maximum applied electric field is on the order of *500 V/cm*, therefore, below the saturation point.

The mobility constant varies with temperature approximately as T^{-m}, where "m" depends on the type of material and on the charge carrier. This dependence becomes crucial for the performance of Silicon drift detectors, as will be discussed in chapter 4.

2.1.2 Intrinsic and doped semiconductors

In a pure semiconductor, the electrons in the conduction band are generated by thermal excitation. Charge concentration is given by:

$$n_i = AT^{3/2} \cdot \exp\left(\frac{-E_g}{2kT}\right) \quad \textbf{(2.2)}$$

where "E_g" is the magnitude of the energy gap, "k" the Boltzmann constant and "A" is the proportionality constant characteristic for each material. For pure Silicon at room temperature, $n_i=p_i=1.45\times10^{10}\ cm^{-3}$. In the equilibrium condition, the number of electrons in the conduction band (n) is equal to the number of holes in the valence band (p). Such a material is called an "intrinsic" semiconductor (subscript "i" in the equation above).

The concentration balance between electrons (n) and holes (p) can be changed by introducing a small amount of impurity atoms that have one extra or one less valence electron in the outer atomic shell. By a process called thermal activation these impurities integrate into the semiconductor lattice and create what is called a doped semiconductor.

Impurities with an extra electron are called "donors". Some of the most commonly used donor elements are Arsenic and Phosphorous. The extra electron will reside in a discrete energy level in the energy gap region but close to the conduction band level (only *0.05 eV* for Silicon). At normal temperatures, the extra electron is easily excited into the conduction band enhancing the conductivity of the material. In such materials, the current is mainly due to electrons, which are called majority carriers. The holes will only contribute to the current as minority carriers. This type of doped semiconductor is called "n-type" semiconductor.

If the impurity has one less electron in the outer atomic shell it is called "acceptor". Boron is the most common acceptor element used in Silicon. In this case, there is an excess of holes. An extra energy band is created in the energy gap region, but this time, close to the valence band level. Electrons in the valence band

are easily excited to this energy level, leaving behind extra holes. Such material is called a “p-type” semiconductor and the holes are the majority carriers.

Usually, the amount of dopant used is very small, 10^{13} *atoms/cm*^{3}, a few parts per billion compared to the Silicon density. However, for electrical contacts, high impurity concentrations can be used. In these cases, the concentrations can be as high as 10^{20} atoms/cm^3. Heavily doped p-type or n-type semiconductors are labeled as “$p+$” or “$n+$” material.

In thermal equilibrium, the concentrations of electron (n) or hole (p) obey a simple law of conservation. Since the semiconductor is neutral, the concentrations of donor (N_D) and acceptor (N_A) must be equal so that,

$$N_D + p = N_A + n \tag{2.3}$$

In an n-type material, $N_A=0$ and $n \gg p$, therefore the electron density is $n \approx N_D$. Analogously in a p-type material the hole density can be approximated by $p \approx N_A$.

In a more quantitative calculation, considering Boltzmann statistics for the number of energy levels in the conduction band populated by electrons, the carrier concentration in doped materials is given by:

$$n = N_D = n_i \exp\left(\frac{E_F - E_i}{kT}\right) \quad \text{for n-type materials} \tag{2.4}$$

and

$$p = N_A = n_i \exp\left(\frac{E_i - E_F}{kT}\right) \quad \text{for p-type materials.} \tag{2.5}$$

where E_i is the intrinsic energy of the semiconductor and E_F is the Fermi energy. The Fermi energy level is defined as the energy level for which the occupation probability is *50%*. So the difference between the intrinsic semiconductor and a doped semiconductor can be seen as a shift of the Fermi energy level with respect to the intrinsic energy level.

2.1.3 Basic p-n junction properties

The p-n junctions are of great importance for understanding semiconductor devices. In the case of the Silicon drift detectors, the cathodes and the detector bulk form a p-n junction that will deplete the Silicon bulk in order to allow the electron drift. The basic theory of current-voltage characteristics of p-n junctions was first established by Shockley [ref. 2.1, 2.2].

When a p-type semiconductor is connected to an n-type semiconductor, there is an abrupt change of carrier concentration. In this case, charge carriers migrate across the junction due to diffusion. The flow of charge from one side of the junction to the other leaves behind a net charge due to the fixed space charge. This will create a net negative space charge on the p-side and a net positive space charge on the n-side of the junction. The accumulated space charge creates an electric field opposite to the charge flow that will oppose further charge diffusion thus creating an equilibrium condition. The region over which the charge imbalance exists is called the “depletion region”, and it extends into the p and n side of the junction.

The depletion region has some important properties as a medium for radiation detection. The electric field of the depleted region removes most of the free charges created near the junction. Electrons are swept towards the n-type material while holes are swept toward the p-type material. Thus, the region is “depleted” of free electrons and holes. The only significant charge remaining in

this region are the fixed lattice charges. Because the fixed charges do not contribute to the conductivity, the depletion region exhibits high resistivity. Radiation passing through the depleted region with sufficient energy will create electron-hole pairs. These charges will be swept out of the depletion region by the electric field before recombination and their motion constitutes a basic electric signal.

2.1.3.1 Depth of the depletion layer

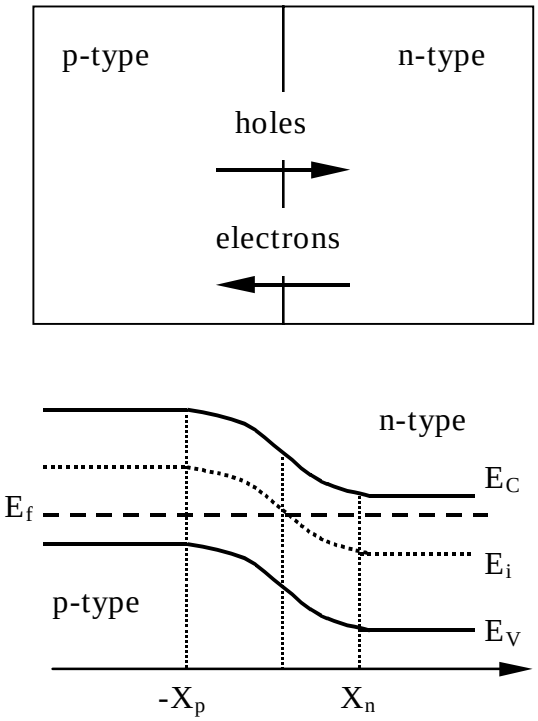

Figure 2.1: *(a) Schematic of the p-n junction, considering the abrupt junction approximation. (b) Energy levels of the two materials in contact.*

For simplicity, we are considering the abrupt junction approximation, where the impurity concentration changes abruptly. In a real p-n junction, there is a finite length, called Debye length, over which the transition takes place. Figure 2.1 shows a schematic view of the p-n junction and the energy levels of the

junction. An important fact is that once thermal equilibrium is established the Fermi level is equal on both sides of the junction, however the electrical potentials such as the conduction and valence band levels (E_C, E_V) are unequal. This can be understood as follows. Initially, the electrons at the conduction band on the n-type material see unpopulated lower energy levels in the p-type material and so they diffuse into them. The developing space charge bends the energy bands of the p-material to a higher level until these levels become inaccessible for electrons.

The zero electric potential level can be defined as:

$$\phi = -\frac{(E_i - E_F)}{q} \tag{2.6}$$

Using equations 2.4 and 2.5, the potential of n-type and p-type material can then be derived as:

$$\phi_n = -\frac{(E_i - E_F)}{q} = \frac{kT}{q}\ln\left(\frac{N_D}{n_i}\right) \tag{2.7}$$

$$\phi_p = -\frac{(E_i - E_F)}{q} = -\frac{kT}{q}\ln\left(\frac{N_A}{n_i}\right) \tag{2.8}$$

The build-in potential of a p-n junction is defined as the potential difference between the p and n side of the junction.

$$\phi_{build-in} = \phi_n - \phi_p = \frac{kT}{q}\ln\left(\frac{N_D N_A}{n_i^2}\right) \tag{2.9}$$

For the Silicon used in the STAR/SVT project, considering a "*n*" doping concentration of $1.0 \times 10^{12}\ cm^{-3}$ and a "p" doping of the cathodes with a concentration of $1.0 \times 10^{18}\ cm^{-3}$, the build-in potential is approximately *0.58 V*.

The electric potential is calculated by solving the Poisson equation:

$$\frac{d^2\phi}{dx^2} = -\frac{dE}{dx} = -\frac{\rho}{\varepsilon} \tag{2.10}$$

where "*E*" is the electric potential and "ε" is the permittivity of the material ($11.7 \cdot \varepsilon_0$ for Silicon). Considering that the depletion layer is from $x=-x_p$ on the p-side of the junction to $x=x_n$ on the n-side of the junction, the electric potential is given by:

$$E(x) = -\frac{d\phi}{dx} = -\frac{qN_A}{\varepsilon}(x + x_p) \quad \text{for } -x_p \le x < 0 \tag{2.11}$$

and

$$E(x) = -\frac{d\phi}{dx} = +\frac{qN_D}{\varepsilon}(x - x_n) \quad \text{for } 0 \le x < x_n \tag{2.12}$$

At the junction, $x=0$, the electric field is maximum.

$$E_{\max} = +\frac{qN_A}{\varepsilon} x_p = +\frac{qN_D}{\varepsilon} x_n \tag{2.13}$$

From the equation above, the thickness of the depletion layer can be written as:

$$W = x_p + x_n = \frac{\varepsilon}{q} E_{\max} \left(\frac{1}{N_A} + \frac{1}{N_D} \right) \tag{2.14}$$

To express the depletion layer as a function of the potential, we calculate the build-in-potential $\phi_{build\text{-}in}$ as the total potential difference from one side of the depletion layer to the other:

$$\begin{aligned}\phi_{build-in} &= -\int_{-x_p}^{x_n} E(x)dx \\ &= -\int_{-x_p}^{0} E(x)dx - \int_{0}^{x_n} E(x)dx \\ &= \frac{qN_A x_p^2}{2\varepsilon} + \frac{qN_D x_n^2}{2\varepsilon} \\ &= \frac{1}{2}E_{\max}\left(x_p + x_n\right) = \frac{1}{2}E_{\max}W\end{aligned} \qquad \textbf{(2.15)}$$

From equation 2.14 and 2.15 the thickness of the depletion layer can be written as:

$$W = \sqrt{\frac{2\varepsilon}{q}\left(\frac{N_A + N_D}{N_A N_D}\right)\phi_{build-in}} \qquad \textbf{(2.16)}$$

2.1.3.2 Reverse biased p-n junction

With no external bias, the build-in potential of the p-n junction does not generate a large enough field to move the electron-hole pairs sufficiently fast for efficient detection. In addition, the thickness of the depletion region is quite small (approximately *28 μm* in the case of the STAR/SVT Silicon drift detector cathode-bulk junction). Therefore, unbiased junctions are not useful for radiation detectors.

The p-n junction performs like a diode when biased. By applying a reverse bias on the p-n junction, virtually all the applied voltage will appear across the depletion region. Electrons from the n-type region will reach deeper into the p-type region, thus the thickness of the depletion region increases. The thickness of

the depleted region can be approximated using equation 2.16 replacing the build-in potential, $\phi_{build\text{-}in}$ by the external bias voltage, V_{bias}.

$$W = \sqrt{\frac{2\varepsilon}{q}\left(\frac{N_A + N_D}{N_A N_D}\right)V_{bias}} \qquad \textbf{(2.17)}$$

In most cases, one side of the p-n junction has a much higher doping concentration than the other side. In the specific case of the STAR/SVT Silicon drift detector, the p-type cathodes are doped much more heavily than the n-type detector bulk, therefore, $N_A \gg N_D$. In this case, the depletion region can be expressed by:

$$W = \sqrt{\frac{2\varepsilon V_{bias}}{qN_D}} \qquad \textbf{(2.18)}$$

If the bias potential is large enough, the depletion layer extends through the whole Silicon bulk thickness. In this state, the Silicon is considered “fully depleted”. For convenient detector operation, a low doping concentration (which corresponds to high resistivity) is desirable in order to utilize a lower voltage for full depletion.

Because of fixed charges that build up on both sides of the junction, the depletion region can be compared to a charged capacitor. By increasing the depletion thickness, the distance between the accumulated charges on both sides of the junction increases and the effective capacitance decreases. Under this assumption, the capacitance per unit area of a p-n junction can be calculated as:

$$\frac{C}{A} = \frac{\varepsilon}{W} = \sqrt{\frac{q\varepsilon N_D}{2V_{bias}}} \qquad \textbf{(2.19)}$$

The electronic noise of a signal output is greatly influenced by the detector capacitance. Small capacitance is desirable for good energy resolution.

2.1.4 Effects of ionizing radiation in semiconductors

For low energy radiation that is fully stopped within the semiconductor, the number of the charge carriers created is approximately proportional to the total energy of the incident radiation. For high energy radiation, the incident particle passes completely through the detector, retaining most of its initial energy, and a signal proportional to *dE/dx* is observed. This is the dominant scenario in heavy-ion and high-energy physics experiments.

High-energy charged particles loose energy in matter primarily by ionization, which generates free electron-hole pairs and phonons (lattice vibrations). In Silicon, the energy necessary to create an electron-hole pair at room temperature is *3.62 eV*. This value is higher than the Silicon energy gap (*1.16 eV*) due to energy loss in the crystal lattice.

A second mechanism of energy loss is through the displacement of atoms from the crystal lattice. However, for an atom to be displaced from the lattice, the energy transfer has to exceed the threshold value (*25 eV* for Silicon) and therefore this mechanism is much less probable than the ionization mechanism. The displacement of lattice atoms creates vacancies in the lattice that will affect the properties of the semiconductor, and it is one of the main radiation damage mechanisms. It is a cumulative effect and therefore important to be considered for long term detector performance.

The mean energy loss per unit length is given by the Bethe-Bloch equation [ref. 2.3, 2.4]:

$$-\frac{dE}{dx} = Kz^2 \frac{Z}{A}\frac{1}{\beta^2}\left[\frac{1}{2}\ln\left(\frac{2m_e c^2 \beta^2 \gamma^2 E_{\max}}{I^2}\right) - \beta^2 - \frac{\delta}{2}\right] \quad \textbf{(2.20)}$$

where E_{max} is the maximum energy transfer achievable in a collision:

$$E_{\max} = \frac{2m_e c^2 \beta^2 \gamma^2}{1 + \frac{2\gamma m_e}{M} + \left(\frac{m_e}{M}\right)^2} \quad \textbf{(2.21)}$$

The last term of equation 2.20 corresponds to the density effect correction. The electric field of the incident particle modifies the original field in the semiconductor resulting in a weakening of the interactions and thus reducing the energy transfer. The parameters of equation 2.20 are listed in the table below:

Symbol	**Value-unit**	**Definition**
$\frac{dE}{dx}$	[eVg^{-1}cm^2]	energy loss
K	0.307 [MeVg^{-1}cm^2]	$4\pi N_A r_e^2 m_e c^2$
m_e	0.510 [MeV]	electron mass
c	2.998×10^8 [m/s]	speed of light in vacuum
z		charge of incident particle
Z	Si: 14	atomic number of medium
A	Si: 28.0855	atomic mass of medium
β	v/c	relative particle speed
γ	$1/\sqrt{1-\beta^2}$	Lorentz boost parameter
I	Si: 172	excitation potential per atomic electron
E_{max}		maximum energy transfer
δ		density effect correction
M		incident particle mass

Figure 2.2 [ref. 2.5] shows the mean energy deposition due to ionization for the indicated particles in Lead (Pb), with scaling to Cu, Al, and C, as a function of incident particle momentum calculated using the Bethe-Bloch equation. The density effect term becomes important in the range of relativistic particles leading

to an independence of the mean energy loss on the incident energy. Particles with this energy loss are called minimum ionizing particles (MIP).

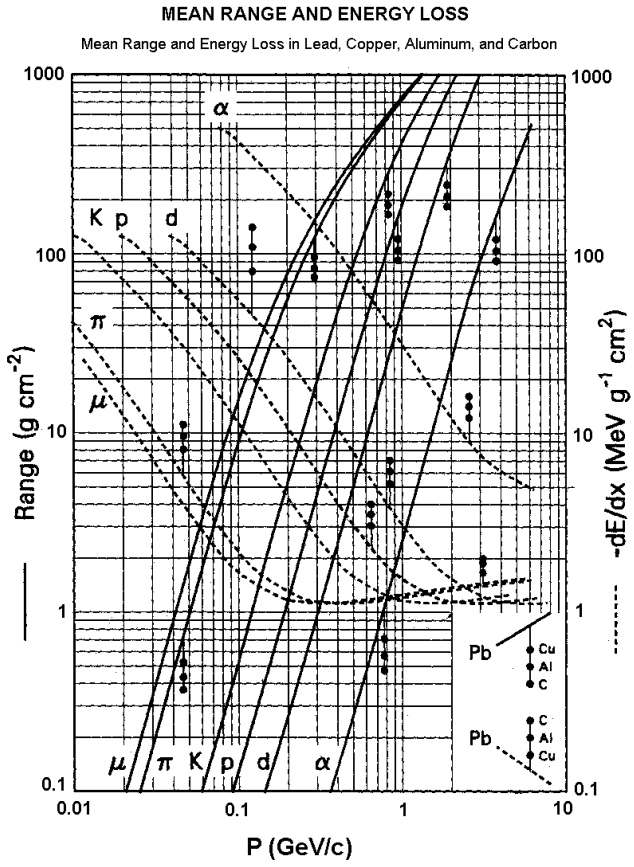

Figure 2.2: *Mean energy deposition (dashed lines) in Lead (Pb), with scaling to Cu, Al, and C, for the indicated particles, calculated from the Bethe-Bloch equation. The solid lines correspond to the equivalent penetration range inside the Lead.*

2.2 Overview of Silicon detectors

Silicon detectors were initially developed for measuring only the energy of the particles. Due to its high stopping power, particles with relatively low energy (up to a few MeV) are completely stopped inside the detector, transferring all their energy into the detection medium which allows a precise measurement of the

particle incident energy. Surface barrier detectors are the most commonly used type of Silicon detector for energy measurements.

Pad detectors were developed to provide a position measurement in addition to the particle's energy, which enables the usage of Silicon devices as tracking detectors. To improve the resolution and reduce the number of readout channels, Silicon strip-detectors were introduced. Due to its characteristics, a strip-detector is ideal to be used as tracking detector in high-energy experiments. In these experiments, the energy range of the particles is already too high for them to be stopped in the detector. However, for particle tracking, it is desirable to minimize the energy loss and avoid interfering with the original particle trajectory, through multiple Coulomb scattering. Therefore, the application of Silicon detectors has changed from energy measuring devices to position sensing tracking detectors. However, the energy loss information can still be used for particle identification (see figure 2.2).

In recent years, two new types of Silicon detectors were introduced, active pixel detectors and drift detectors. Both combine high spatial resolution with cost-effective electronics solutions leading to sophisticated tracking and vertexing detectors. The development of a Silicon Drift Detector, its characteristics and application are the main subjects of this thesis.

2.2.1 Surface Barrier Silicon detector (SBSD)

Probably the most commonly used detector for charged particle measurements is the Surface Barrier Detector. It consists of a junction, formed between the Silicon and a metal (n-type Silicon with Gold), with properties similar to a p-n junction. By biasing the detector, the depletion zone extends through the entire thickness of the Silicon wafer thus increasing the detection region. Surface Barrier detectors have excellent energy resolution, but do not provide position

information. They are produced in a variety of thickness' and shapes. Figure 2.3 shows a schematic of a Surface Barrier Silicon Detector.

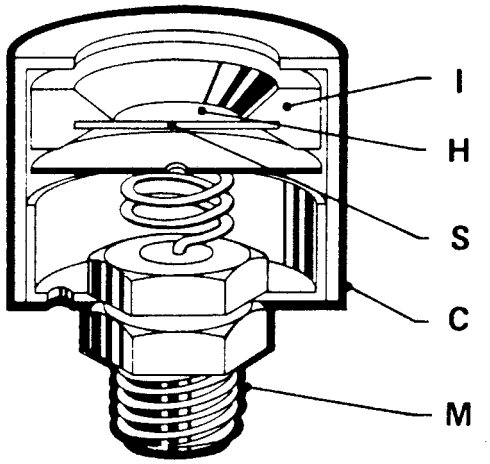

Figure 2.3: *Schematic of a Surface Barrier Silicon Detector. The circular Silicon wafer (S) is mounted in an insulating ring (I) whose back and front surfaces are metallized. (c)- grounded metal case, (M)- BNC connector.*

2.2.2 Pad detector

Pad detectors consist of arrays of separate discrete Silicon diodes implemented on the same Silicon wafer [ref. 2.6]. Each independent diode pad is connected to an individual readout channel through a surface routing on the detector substrate, see figure 2.4. The number of readout channels is proportional to the detector area. The position resolution is determined by the pad size, therefore, a higher position resolution requires a higher number of pads and readout channels which is the main disadvantage of this type of detector.

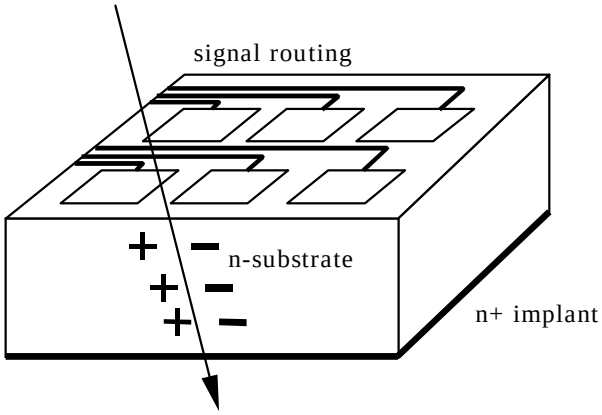

Figure 2.4: *Schematic view of a pad detector.*

2.2.3 Microstrip detector

Microstrip detectors are composed of separate readout strips, usually in steps between *10* to *50 μm*, and several centimeters long [ref. 2.7, 2.8]. Figure 2.5 shows a schematic diagram of the detector. In addition to the particle energy it provides one-dimensional position information. The position resolution is determined by the distance between strips (pitch) which can be theoretically as small as *1 μm*, however, the high cost for the appropriate number of readout channels prohibits such small pitch. To reduce the number of readout channels, a capacitive charge division method is used that allows wider strip separation, up to *60 μm*. By calculating the center of gravity of the charge collected, the position of the particle track can be determined down to a *5 μm* resolution.

Due to the small thickness of the depleted Silicon wafer (around *300 μm*), the response time of this type of detector is relatively fast. Charge collection can be performed in less than *10 ns*, allowing these detectors to be used as triggering devices or to be used in high luminosity experiments.

To measure two-dimensional information, several layers of tilted microstrip detectors can be used. But, due to position ambiguities, the maximum resolvable track density is limited. Double-sided microstrip detectors that can provide two-dimensional information in a single layer were developed to reduce the radiation length for tracking detectors. However, the number of readout channels remains the same as for two single sided layers.

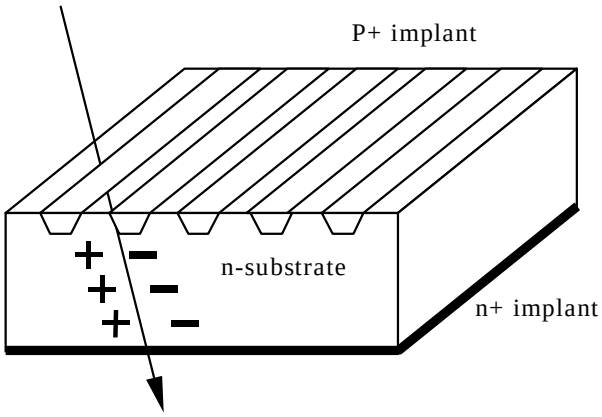

Figure 2.5: *Schematic view of a single sided micro-strip detector.*

Microstrip detectors were originally used as vertex detectors in fixed target experiments searching for decays of charm particles. Due to their advantages over multi-wire gas chambers, microstrip Silicon detectors were furthermore applied in high luminosity collider experiments. With this new trend, the microstrip detector development has shifted from aiming to achieve high position resolution with minimal detector thickness to aiming to cover very large areas with low number of output channels (*5* m^2 for D0 experiment and *40* m^2 for ATLAS experiment [ref. 2.9]), by still maintaining high resolution and minimal scattering cross section.

2.2.4 CCD

CCD detectors (Charge-Coupled Device) [ref. 2.10, 2.11] consist of a square matrix of potential wells, achieved by mounting a two-dimensional array of

MOS capacitors on a Silicon wafer. Signal charges generated by the passage of particles or by illumination are collected in this matrix of potential wells. The signal readout is performed by shifting the collected charge from pixel to pixel, in parallel, from row to row. Thus, the CCD image is converted from a two-dimensional charge pattern to a serial train of pulses, in an unambiguous manner. Figure 2.6 shows the basic principle of the operation of a CCD detector.

The largest use of CCD detectors is for imaging cameras. With the invention of the buried-channel architecture for CCD's, where the charge is accumulated below the surface instead of in the Si-SiO_2 interface, this type of detector became more useful for scientific applications [ref. 2.12]. The fact that CCD detectors can be relatively thin (*180 μm* thick), leads to less multiple Coulomb scattering and less X-ray background, which makes this technology attractive for tracking detectors.

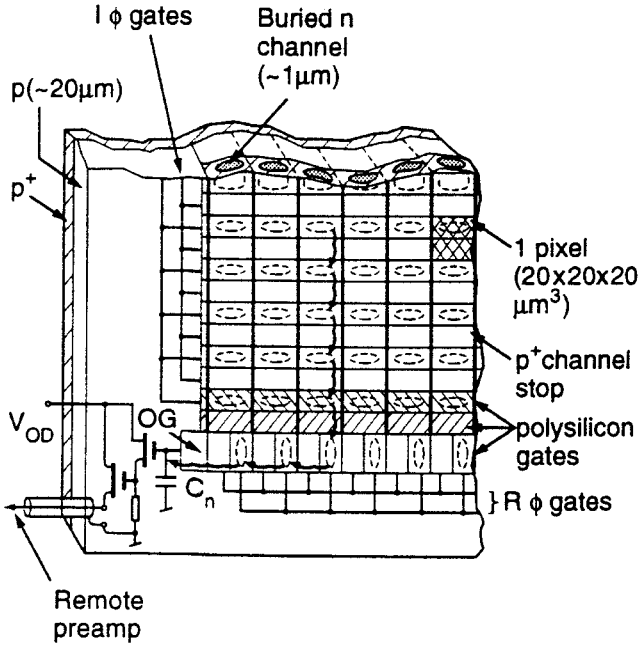

Figure 2.6: *Basic operation principle of a CCD detector.*

Due to the slow readout (on the order of *ms*), this type of detector is not appropriate for high rate experiments. In addition, radiation damage affects greatly the properties of the surface interfaces and junctions, altering the potential distribution in that region. Because CCD detectors store the charge near the surface, they are more susceptible to radiation damage and therefore inappropriate for use in long duration high rate experiments.

CCD's are presently used in the SLD experiment at SLAC Linear Collider in the upgraded vertex detector [ref. 2.13]. 96 two-dimensional CCD's with a total of 307 Mpixel were arranged in three concentric cylinders surrounding the e^+e^- collision point.

2.2.5 Active pixel detector

Active pixel detectors (APD) consist of a matrix of contiguous particle sensing detectors with dimensions between $30\ \mu m$ and $500\ \mu m$ [ref. 2.14, 2.15]. Each sensor element has an associated signal processing circuit that is connected directly to the detecting substrate. Two types of APDs were developed: the monolithic APD that has the readout circuit inside the detection substrate separated by a SiO_2 layer [ref. 2.16], and the hybrid APD that has the electronics mounted on a separate layer connected by bump bonds (see figure 2.7). Both provide two-dimensional coordinate information, like CCD and pad detectors. The advantage of this type of detector compared to pad detectors is the fact that the readout electronics is mounted directly on the detector, providing a more robust and compact detector. Also, the input capacitance for the readout electronics is relatively lower, therefore reducing the electronic noise levels. The advantage of this type of detector over a CCD type detector is its fast gating speed. Unlike the CCD it does not require to latch the signals. Also, active pixel detectors are less susceptible to radiation damage.

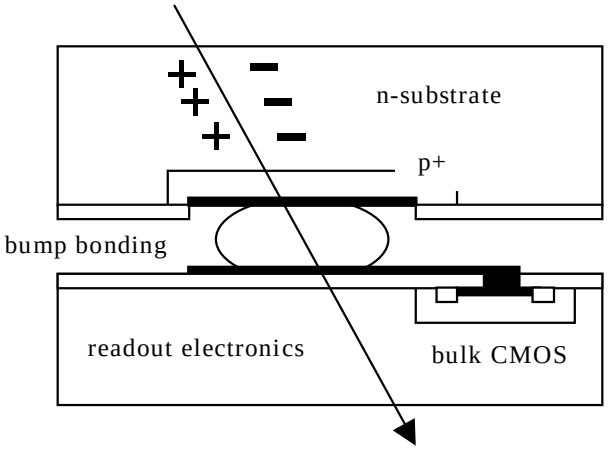

Figure 2.7: *Schematic view of one pixel of a hybrid type active pixel detector.*

At this time, the major problem with APD's is their production yield. The bump bonding is a complicated and delicate process that generally lowers the production yield considerably. Active pixel detectors are at a relatively early stage of development and they are demonstrating their capability in test beams and in fixed target experiments as general tracking detectors. A telescope detector with 9 active pixel planes was implemented in the CERN Heavy Ion experiment WA97. A 100 Mpixel detector is expected to be build for the inner tracking detector for the ATLAS experiment [ref. 2.14] at the LHC (Large Hadron Collider).

2.3 Silicon drift detectors

To use Silicon detectors as tracking devices, it is desirable to cover as large an area as possible, with good position resolution, and yet, with a minimum cost. Traditional position sensing Silicon detectors such as microstrip detectors or pixel detectors can provide relatively large area coverage and good position resolution. However, the number of readout channels increase proportionally with coverage and position resolution. In search for a more cost effective detector, that can

satisfy both requirements, a new kind of detector was proposed by Gatti and Rehak [ref. 2.17], namely a solid state drift chamber.

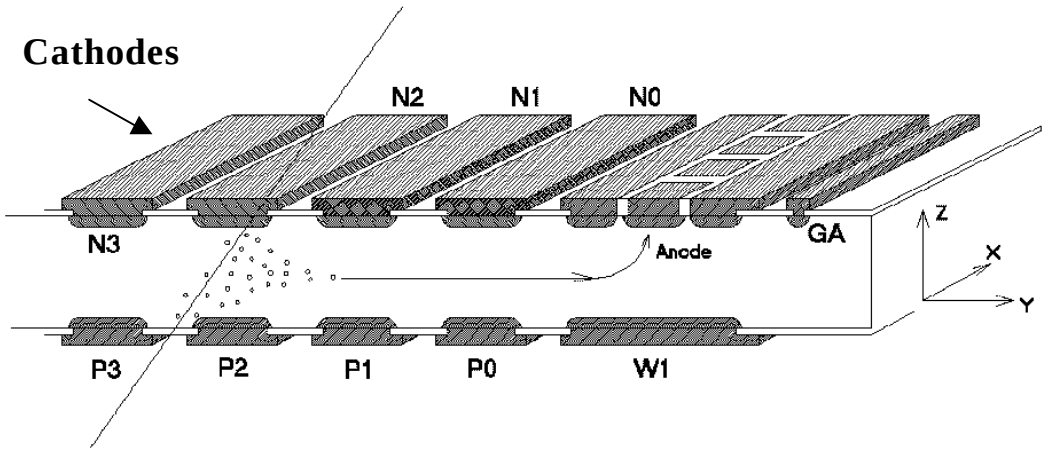

Figure 2.8: *Schematic of Silicon drift detector and its operation.*

This Silicon drift detector is capable of providing position and ionization measurements with a reduced amount of electronics. Its principle is based on creating a drift channel inside a depleted Silicon wafer, thereby combining the advantages of a semiconductor detector with some of the best features of gas drift chambers, such as low number of input channels. Figure 2.8 shows the basic idea of a Silicon drift detector. An ionizing particle passing through the Silicon detector creates electron-hole pairs. With an electric potential field, applied by the cathodes, the electrons are forced to drift towards the edge of the detector where collection anodes are placed. By measuring the drift time together with the distribution of signals along the readout anodes, position information can be obtained in both dimensions.

Charge sharing across several anodes due to diffusion plus Coulomb repulsion during the drift leads to high position resolution with a relatively low number of readout channels. Small anode input capacitance allows a reduction in the electronics noise levels.

References

[2.1] W. Shockley, "The theory of p-n junctions in semiconductors and p-n junction transistors", *Bell Syst. Tech. J.*, **28**, 435 (1949); *Electrons and Holes in Semiconductors,* D. Van Nostrand, Princeton, N. J., 1950.

[2.2] C. T. Sah, R. N. Noyce, and W. Shockey, "Carrier Generation and Recombination in p-n junction and p-n junction characteristics", *Proc. IRE,* **45**, 1228 (1957).

[2.3] G. Hall, "Ionization Energy losses of highly relativistic charged particles in thin Silicon layers", *Nucl. Inst. and Meth.*, **220** (1984) 356-362.

[2.4] J.F. Bak, *et al.*, "Large Departures from Landau distributions for high-energy particles traversing thin Si and Ge targets", *Nucl. Phys.*, **B288** (1987) 681-716.

[2.5] Review of Particle Properties - Particle Data Group, *Phys. Lett.*, **B170** (1986) 1-350.

[2.6] E. Laegsgaard, *Nucl. Inst. and Meth.*, **162** (1979) 93.

[2.7] B. Hyams, *et al.*, *Nucl. Inst. and Meth.*, **205** (1983) 99.

[2.8] C. Colledani, *et al.*, "A submicron precision Silicon telescope for beam-test purposes", *Nucl. Inst. and Meth.*, **A372** (1996) 379.

[2.9] ATLAS, Technical Proposal for a general-purpose pp experiment at the Large Hadron Collider at CERN, CERN/LHCC/94-43.

[2.10] W. S. Boyle and G. E. Smith, *Bell Syst. Tech. Journal*, **49** (1970) 587.

[2.11] R. H. Walden, *et al.*, *Nucl. Inst. and Meth.*, **51** (1972) 1635.

[2.12] C. J. S. Damerell, *et al.*, *Nucl. Inst. and Meth.*, **185** (1981) 33.

[2.13] C. J. S. Damerell, *et al.*, "Design and performance of the SLD vertex detector: a 307 Mpixel tracking system", *Nucl. Inst. and Meth.*, **A400** (1997) 287-343.

[2.14] P. Middelkamp, "Tracking with active pixel detectors", Thesis at Fachbereich Physik Bergische Univ., Germany, (1996).

[2.15] E. H. M. Heijne, P. Jarron, "Development of Silicon pixel detectors", *Nucl. Inst. and Meth.*, **A275** (1989) 484.

[2.16] G. Vanstraelen, “Monolithic integration of solid-state particle detectors and readout electronics on high resistivity Silicon”, Thesis at the Katholieke Univ. Leuven, Belgium, (1990).

[2.17] E. Gatti and P. Rehak, Semiconductor Drift Chamber – An Application of a Novel Charge Transport Scheme, *Nucl. Inst. and Meth.*, **255** (1984) 608.